Lab on a Chip

RSC Publishing

PAPER

View Article Online
View Journal | View Issue

Cite this: *Lab Chip*, 2013, **13**, 1724

A scalable approach for high throughput branch flow filtration

David W. Inglis*[a] and Nick Herman[b]

Received 11th February 2013,
Accepted 28th February 2013

DOI: 10.1039/c3lc50192b

www.rsc.org/loc

Microfluidic continuous flow filtration methods have the potential for very high size resolution using minimum feature sizes that are larger than the separation size, thereby circumventing the problem of clogging. Branch flow filtration is particularly promising because it has an unlimited dynamic range (ratio of largest passable particle to the smallest separated particle) but suffers from very poor volume throughput because when many branches are used, they cannot be identical if each is to have the same size cut-off. We describe a new iterative approach to the design of branch filtration devices able to overcome this limitation without large dead volumes. This is demonstrated by numerical modelling, fabrication and testing of devices with 20 branches, with dynamic ranges up to 6.9, and high filtration ratios (14–29%) on beads and fungal spores. The filters have a sharp size cutoff (10 × depletion for 12% size difference), with large particle rejection equivalent to a 20th order Butterworth low pass filter. The devices are fully scalable, enabling higher throughput and smaller cutoff sizes and they are compatible with ultra low cost fabrication.

1.0 Introduction

Separation of particles by size is an essential step in environmental assays, biochemical analysis and numerous industrial and biomedical processes. Filtration, sedimentation and centrifugation techniques are frequently used to separate and classify particles, but performance is generally poor when particle size and the difference in size between target and non-target particles are small.[1] Furthermore, clogging and fouling of device components is inevitable. The development of microfluidics in the past 15 years has led to a number of new methods for the separation and selection of micro-particles through precise control of fluid flow; these have been applied to cells, polymer beads, bacteria, spores, organelles, and bio-macromolecules.[2] In contrast to membrane filtration and its variants, these continuous flow microfluidic filtration methods separate particles that are smaller than the minimum pore or feature size, enabling continuous, clog-free operation. However these methods are unable to deliver a sharp particle size cutoff at a dynamic range greater than 5, while filtering a large fluid flow. Thus, despite continuing progress, the central problem of continuous flow separation science is avoiding clogs while maintaining a precise separation size a high volume throughput.

In this work we have been able to achieve precise filtration at large fluid flow through the judicious optimization of the branched flow fractionation (BFF) approach. Fung described the fundamentals of BFF in 1973[3] in the context of depletion of red blood cells from small capillaries. More recently its usefulness for hard particles has been demonstrated by Yamada and Seki.[1,4] Since then a number of microfluidic "plasma skimming"[5] devices based on this principle have been demonstrated.[6–9] BFF separates small from large particles because small particles can flow in streamlines that are closer to a boundary than large particles. Assuming that particles do not affect streamlines and are geometrically restricted away from walls by a distance equal to their radius, the cutoff size is determined by the width of the boundary layer in the main channel that is drawn up into each branch (Fig. 1(a) inset). This is a frequent assumption in the microfluidic particle separation literature, that is not always true,[10] but it provides a suitable starting point for the design process.

BFF is ideal for achieving a large dynamic range because increasing the length of a branch while keeping other parameters constant (such as applied pressure and feature size) increases the hydraulic resistance of the branch, reducing the fluid flow down the branch. This reduces the width of the boundary layer that will flow down the branch and the size of particles that can enter the branch. This, in turn, makes it possible to separate nanoscale particles with low-cost, micro-scale features. Furthermore, the main channel can be made arbitrarily large, enabling the passage of very large particles, leading to an extremely large dynamic range and a greatly reduced risk of clogging. The cost of a large dynamic range (separating very small particles) and using a large main

[a]*Department of Physics and Astronomy, Macquarie University, NSW, 2109, Australia. E-mail: david.inglis@mq.edu.au; Tel: +612 9850 7747*
[b]*BTF Pty Ltd, North Ryde, NSW 2113, Australia*

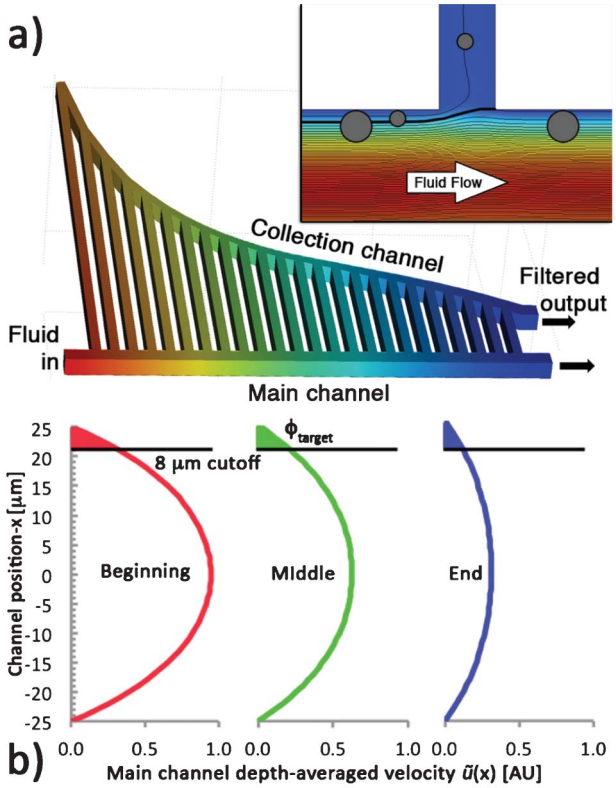

Fig. 1 Example geometry of a BFF device where multiple branches connect to a single output. Colour represents pressure in the device (red = 1, blue = 0). Inset: illustration of the fractionation principle whereby large particles are excluded from a branch, colour represents flow speed. (b) Depth-averaged flow speed *versus* channel position at three representative points along the main channel.

channel is that a very small fraction of the input fluid flow is filtered *i.e.* most of the fluid flows down the main channel and is unaffected by filtration. The only way to overcome this is to use many branches. The problem with this is highlighted, for example, in Xue *et al.*,[11] who evaluated BFF designs having 10 cylindrically symmetric branch points using CFD (computational fluid dynamics). They proposed 6 designs where branches connected a central input channel to a large concentric collector. These designs do not deliver a sharp size cutoff, as their best device showed variation in size cutoffs by 50%, and all have large dead volumes in the large-volume, concentric collector. Large dead volumes are undesirable because they set a lower limit on the volume of sample that can be processed and, since devices must be wet prior to operating, dilute the filtered product.

A similar problem was described by Sethu *et al.*[12] They fabricated 500 small-pore, high-resistance filter elements along the side of a main channel, and varied the shape of the collection channel to cause equal fluid flow at each pore. Two channel geometries were proposed and assessed by CFD. However, in their geometries, the desired equal fluid flow down each element could not be achieved and the best result varied by approximately 25%. These two examples (ref. 11,12) highlight the difficulty of the problem that we have solved.

The need for a new approach becomes clear when considering how to connect a very large number of branches (>50) to a large main channel where each must have the same cut-off size. These branches necessarily intersect the main channel at different points along the main channel, yet must terminate at a common, 0-pressure outlet. The pressure dropped along the first branch will be greater than the pressure dropped along the last branch because the pressure in the main channel decreases along its length. If the total fluid withdrawn from the main channel is small then the branches must have different lengths if they are to carry the same fluid flow. We ask, how should the length of these branches be calculated.

In a more practical case, the total amount of fluid withdrawn from the main channel is significant. Now the pressure drop in the main channel is non-linear and calculating the length of each branch is further complicated. Analytical approaches that use an electrical resistor network are attractive, but have so far failed us, as discussed later. The present paper provides a universally applicable approach to overcome this challenge.

2.0 Design and methods

Our goal is to produce a compact network of microfluidic channels that split an incoming fluid stream into two outgoing streams, one of which has been depleted of large particles (filtered). Such a continuous flow filter must have one input and two outputs. The ratio of the filtered to the total volume throughput, defined as the filtration ratio, F_R should be high. This device should also have a large dynamic range and a sharp size cut-off.

An example BFF device proposed and investigated in this work is shown in Fig. 1(a). Fluid comprising a mixture of various size particles enters the main channel on the left. Some fluid flows up into branches to a collection channel carrying particles that are below the cutoff size. The collection channel accumulates the filtered product of each branch, while the main channel flow rate decreases in the same proportion. These multiple branches enable an increase in the filtration ratio over what can be achieved with a single branch. In order for this device to function optimally we need to determine the length of each branch and what shape the collection channel should have to deliver the same cutoff size at each branch.

2.1 Device design by iterative finite element analysis

Our device designs were produced by iteratively changing an initial geometry and solving each iteration using 3D finite element analysis of incompressible, steady-state, Navier–Stokes equations in COMSOL.

2.1.1 Design constants and initial conditions. We first define device features that are constant throughout our iterative process. At all stages of iteration the devices have the minimum feature size, Δ = 25 μm. Branches have a constant width $W = \Delta$, and for device compactness, branch

spacing of Δ. The device depth is 2Δ, due to the limitations of our fabrication process. We select the number of branches (N = 20) and the width of the main channel (W = 50 μm). The main channel has a length of 2ΔN + 5Δ, 3Δ upstream of the first branch and 2Δ downstream of the last section to allow fully developed flow to form between model boundaries and branch points. The pressure at the input is 1 Pa and is 0 Pa at both outlets, giving an pressure drop per unit length, G, of 1/(2ΔN + 5Δ) [Pa μm^{-1}]. We specify that the width of the collection channel starts at Δ and grows to 2Δ, according to the formula $W = \Delta\left(1 + \frac{n}{N}\right)^2$, where n is the branch number. Increasing the width of the collection channel in this nonlinear fashion was found to produce solutions with lower dead volume than linearly growing the collection channel width. Finally we force the last segment of the collection channel to be parallel to the main channel.

The initial condition in our iterative design is the length of the branches, $f_0(n)$, which specifies length at the left edge of each branch. It is arbitrarily chosen to be the line $f_0(n)$ = 800 − 35n μm. The initial geometry of the device is shown in Fig. 2(a). The 3D Navier–Stokes equation is then numerically solved using COMSOL giving the fluid velocity field everywhere (Fig. 2a).

2.1.2 Iteration. Each iteration step j of our design process involves calculating a new discrete function $f_j(n)$ which determines the length of each branch at this step. We now provide the criteria used to determine $f_j(n)$. This criteria compares the actual flows in each of the branches at this iteration step with their respective target flows. Subsequent to that their lengths are adjusted to bring these flows closer to their targets. If the flow is higher than the target flow, the branch is lengthened and if the flow is lower than the target, the branch is shortened.

In order to determine the target flows we first calculate the amount of fluid from the main channel drawn by the first branch required to yield the desired cutoff size R_c. Here we assume that a boundary stream width of R_c drawn into a branch gives a cutoff size of R_c. This fluid flux is calculated by integrating the analytical solution to the Navier–Stokes equation for incompressible, time independent flow in our main channel. The integration is carried out from $W/2 - R_c$ to $W/2$, (21 to 25 μm in Fig. 2b)) on the depth-averaged velocity, $\tilde{u}(x)$, in a rectangular channel ($d \times w$) with pressure drop per unit length G and viscosity η [see ref. 17 eqn (15)].

$$\tilde{u}(x) = \left(\frac{Gd^2}{12\eta}\right)\frac{96}{\pi^4}\sum_{l=0}^{8}\frac{1}{(2l+1)^4}\times\left\{1 - \frac{\cosh[(2l+1)\pi x/d]}{\cosh[(2l+1)\pi w/2d]}\right\} \quad (1)$$

Consequently, the target flux to achieve the cutoff size R_c for the first branch $\phi_{\text{target}}(1)$ is:

$$\phi_{\text{target}}(1) = \left(\frac{Gd^2}{12\eta}\right)\frac{96}{\pi^4}\sum_{l=0}^{8}\frac{1}{(2l+1)^4} \times \int_{\frac{W}{2}-Rc}^{\frac{W}{2}}\left\{1 - \frac{\cosh[(2l+1)\pi x/d]}{\cosh[(2l+1)\pi w/d]}\right\}\mathrm{d}x \quad (2)$$

Now we determine the target flux for each subsequent n-th branch $\phi_{\text{target}}(n)$ using the same principle but noticing that the depth averaged velocity $\tilde{u}(x)$ scales linearly with pressure and therefore fluid flow rate.

If 2% of the main channel flow is to be extracted by the first branch, the main channel depth averaged fluid flow profile at the 2nd branch is 98% of what it was. The depth averaged velocity $\tilde{u}(x)$ at the second branch is assumed to have the same shape as it did at the first branch but scaled by a factor of 0.98.

To keep the same extraction width (black line in Fig. 1b) we must then extract 2% of this flow. Thus we can state that for each branch to have the same cut-off size, each bifurcation should have the same ratio of branch flow to main channel flow. Since the main channel flow decreases as fluid enters the branches, the target flux for the branches must also decrease. Mathematically the target flux for each subsequent n-th branch $\phi_{\text{target}}(n)$ is then given by:

$$\phi_{\text{target}}(n) = \frac{\phi_{\text{target}}(1)}{\phi_{\text{M}}(1)} \times \left[\phi_{\text{M}}(1) - \sum_{i=1}^{n-1}\phi_{\text{branch}}(i)\right] \quad (3)$$

The main channel flux at the first branch of the model, $\phi_{\text{M}}(1)$, is determined by integrating the fluid velocity on the input boundary of the COMSOL solution. The flow down each branch, $\phi_{\text{branch}}(i)$, is calculated from the velocity at the centreline of each branch also from the COMSOL solution. Which is then converted from a velocity (m s^{-1}) to a flux (m^3 s^{-1}) using the analytically derived (eqn (1)) ratio of maximum

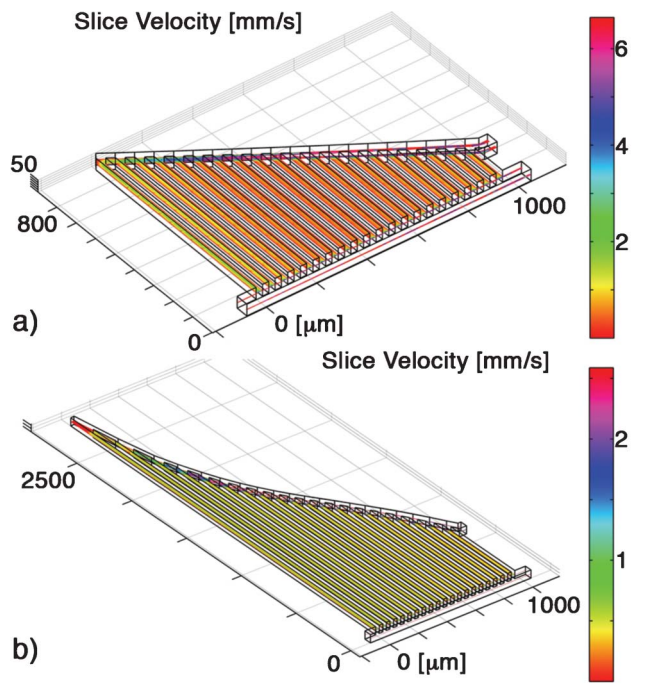

Fig. 2 First and last COMSOL solutions created while iterating toward the 8 micron cutoff device: (a) The initial geometry (j = 0), and (b) when uniformity in cutoff size at each branch has stopped improving (j = 13). To highlight differences in branch flows, the scale range is 0 to 4 times the centreline velocity in the first branch, this puts the main channel flow out of range.

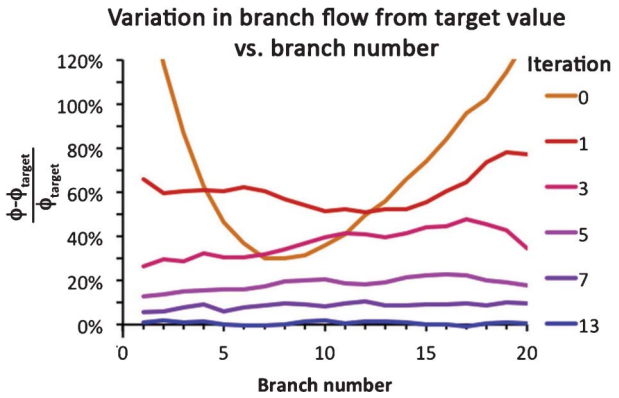

Fig. 3 Variation in branch flow (φ) from the target value (φ_{target}) for each branch at 6 steps in the iteration process. Initial and final, optimised geometries are shown in Fig. 2.

fluid speed (centreline speed) to mean fluid speed (here, for a 50 μm by 25 μm channel this ratio is 1.99). The total flux is the product of the average speed, width and depth.

We now compute the relative difference between target and actual flows as:

$$= \frac{\phi_{branch}(n) - \phi_{target}(n)}{\phi_{target}(n)}$$

When this number is larger than 0, there is too much fluid flow down the branch, the cutoff size is too large, and the branch, $f_j(n)$, is too short. When this number is smaller than 0 there is too little fluid flow, the cutoff size too small, and the branch, $f(n)$, too long. (The top curve in Fig. 3 shows the calculated relative differences between actual and target flows at our initial stage j = 0, these are in the order of 30–120%.) With this information for each branch we now create a new function $f_{j+1}(n)$ where we adjust the lengths of each branch according to the formula:

$$f_{j+1}(n) = f_j(n) \times \left(1 + 0.4 \frac{\phi_{branch}(n) - \phi_{target}(n)}{\phi_{target}(n)}\right) \quad (4)$$

The damping factor of 0.4 provides the fastest convergence. This iteration process is repeated until the relative difference between targets and actual flows is minimised. Fig. 3 shows how the differences in branch flows are reduced with each iteration. Fig. 2(b) shows the geometry when the process stopped after 13 iterations (the normalized sum of squares error is <1.7%). For this final solution we obtain the filtration ratio, F_R, defined as the filtered output flow rate divided by the input flow rate.

Modelling was performed on a 16GB RAM Quad core Xeon™ processor node running COMSOL Multiphysics V3.5a. Models with up to 2 million degrees of freedom were solved, limiting the cutoff size to greater than one fifth of Δ, at twenty or fewer branches.

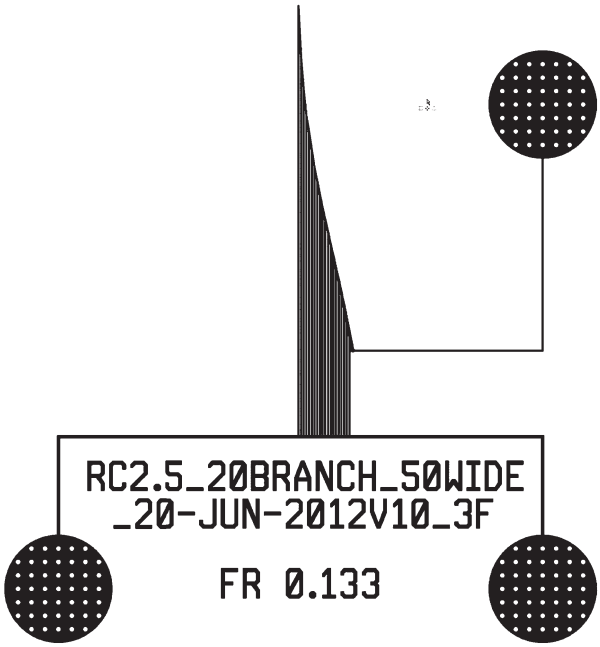

Fig. 4 Layout for 5 μm cutoff size device. Spacing between pads is 9 mm. Bottom left is input, upper right is filtered output.

2.2 Device layout

Coordinates specifying the upper and lower boundary of the collection channel are used to plot a layout in L-Edit (Tanner EDA, California), eliminating the need to draw multiple, individually calculated, branch channels. The filtration ratio is used to calculate channel lengths that must connect to ports on a 9 mm grid and have equal pressure drops across them. Fig. 4 shows a layout of the device with a design cutoff diameter (D_c) of 5 μm and a filtration ratio, F_R, of 13.3%. Three devices were independently designed, developed and tested. Each has 20 branches, and a 50 μm by 50 μm main channel. The minimum feature size in each is 25 μm and the design depth is 50 μm. Table 1 gives the predicted filtration ratio for each device.

2.3 Device fabrication

Devices were fabricated by conventional SU-8 (Gersteltech GM1070) lithography and PDMS (polydimethyl siloxane) on 3″ silicon wafers. The measured depth of the SU-8 mold was 48 μm. Glass-PDMS devices as described earlier[14] were reversibly sealed to glass lids. Devices were wet by immersing in water inside a bell jar, which was evacuated to −97 kPag.

2.4 Experimental setup and analysis

Mixtures of polymer microbeads were created in a 6.5% NaBr solution (to slow sedimentation in tubing) with 0.01% Tween 20 (both chemicals from Sigma Aldrich Australia). 4.2, 5.3, 5.7 (or 6.3), 7.3, 8.3, 9.9 and 15.5 μm diameter fluorescent and non-fluorescent beads (Polysciences and Bangs Laboratories) were added to an approximate concentration of 10^6 per ml each (approximately 0.035% solids net). Fluid pressure was set at 300 mbar (4.4 psi) by a Fluigent Maesflow. Output fractions

Table 1 Comparison of design and measured values. ± values are CV over 3 runs

Design D_c [μm]	Design F_R	Measured F_R ± CV	Cutoff diameter D_c [μm]	Flow rate [μl min^{-1} atm^{-1}]
5.0	13.3%	14.5 ± 0.2%	7.2	93 ± 4
6.0	18.3%	20.4 ± 0.5%	8.9	70 ± 9
8.0	28.4%	28.5 ± 0.4%	9.7	64 ± 10

of at least 20 μL were collected and weighed to determine flow rate and filtration ratio. Devices were disassembled cleaned and re-used. The change in concentration was determined by adding a known volume of a known concentration of 1.9 μm fluorescent beads to each sample prior to analysis by flow cytometry.

2.5 Spore preparation and experiment

A lawn of *A. brasiliensis* NCPF 2275 was grown on Dichloran Rose Bengal Chloramphenicol agar (Oxoid PP2233) by inoculating from a frozen working stock and incubating the agar for five days at 37 °C. After incubation the spores were harvested by wiping the surface of the agar with a sterile cotton swab which is then rinsed in 0.9% saline solution to retrieve the spores. These spores were filtered through a 20 μm nylon mesh filter and diluted to 0.05% w/v in saline containing 0.2% Tween 20. All experiments involving viable Aspergillus spores were conducted within a PC2 (physical containment level 2) laboratory. The harvesting of large numbers of spores from agar plates was done within a Class 2 Biological Safety Cabinet in order to contain any potential airborne particles created during the process. Spores were run in devices for 12 min at 300 mbar.

3.0 Results

3.1 Characterisation of filtration

Fig. 5 shows a false-colour time-lapse fluorescence micrograph of beads flowing through the 8 μm cutoff size device. As fluid is withdrawn from the main channel by successive branches the bright trace from the 10 μm particle moves upward and across, but still within, the main channel. By the twelfth branch it has begin to interact with the branches but does not flow down them. Less bright 6 μm particles can be seen streaking slowly down the branches. This image confirms that the device works as expected. Naturally, the fluid speed in the branches is much lower than that in the main channel and their ratio increases as the cutoff size of the device decreases.

A more complete measure of device performance is provided by measuring the change in micro-bead concentration in the filtered output relative to the input concentration. Fig. 6 shows the ratio of bead concentration in the filtered output divided by the input concentration for three devices. If 0 events were recorded we used 0.5 for purposes of plotting on the log scale. In this Figure we see that the 5 μm device weakly depletes the 7.3 μm beads, strongly depletes the 8.3 μm beads and very strongly depletes the 10 and 15.5 μm beads. The 6 μm device depletes the 10 μm beads by about 10 fold and strongly depletes 15.5 μm beads. The 8 μm device significantly depletes the 15.5 μm beads only. A concentration change of 0.001 is approximately the limit of detection for 15.5 and 9.9 μm beads as there are generally 1000 of these events in our input sample data.

To determine the actual cut off sizes for the three devices we have fitted the data using an *i*-th order Butterworth filter, a common low pass filter in electrical engineering with a simple transfer function. We have not fitted the 15.5 μm bead data as it is at the sensitivity limit. The transfer function (gain *vs.* frequency) for the n-th order Butterworth filter is given by:

$$G(\omega)\frac{G_0}{\sqrt{1+\left(\frac{\omega}{\omega_c}\right)^{2i}}}$$

For our purposes we can replace frequency, ω, with particle diameter, D, and the cutoff frequency, ω_c with the cutoff diameter, D_c. To correctly capture the sharpness apparent in the data we use $i = 20$ for all three devices. This sharpness can also be expressed as a 10× depletion when particle size is 12% larger than the cutoff size. For each device we have then determined a cutoff diameter by least squares fitting. The cutoff diameters are shown in Table 1. This is a universal approach to determine the order and cutoff diameter of a filter

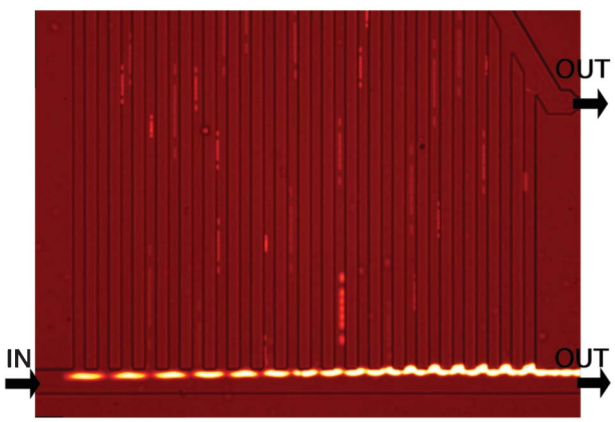

Fig. 5 Time-lapse fluorescence micrograph of a bead mixture flowing through the 8 μm cutoff device. The bead mixture enters at the bottom left, smaller particles (6 μm) enter the vertical branches, while a single large particle (10 μm) is excluded from the branches. The top output is the filtered sample. Note that in this image the pressure and flow speed were significantly lower than typical run conditions.

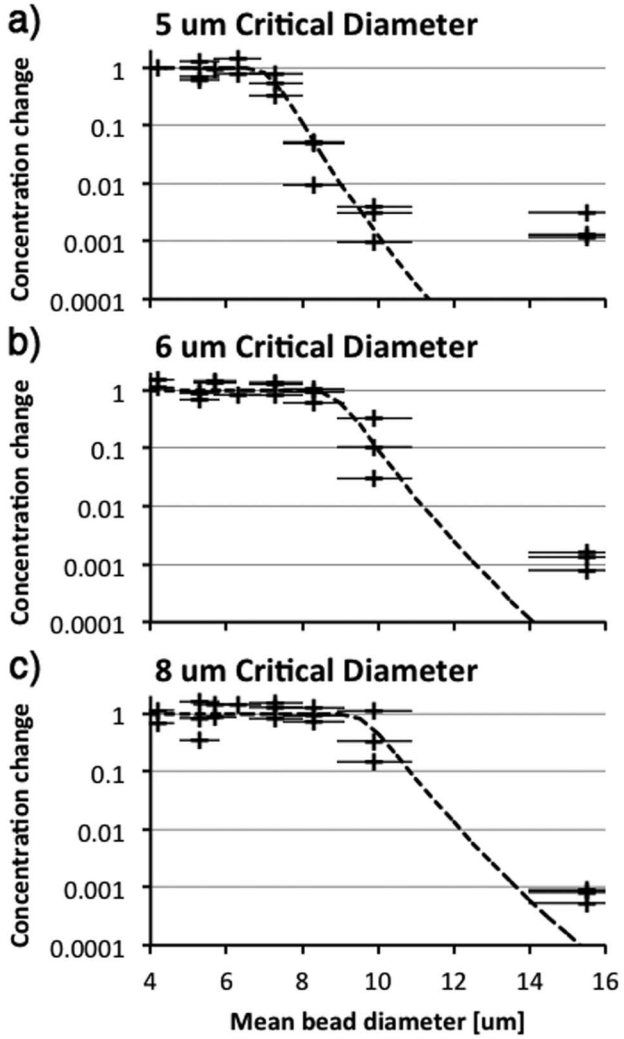

Fig. 6 Change in bead concentration at the filtered output *versus* nominal bead diameter for three different designs (a) 5, (b) 6 and (c) 8 μm cutoff diameter. Error bars show ±10% bead size (typical distribution). Dashed line fit using a 20th-order Butterworth low pass filter transfer function.

and thus to specify the effectiveness of a particle separation system.

The experimentally observed cutoff diameters are significantly higher than the cutoff sizes determined from our design process. This is in agreement with Doyeux *et al.*[10] who showed that contrary to the situation in the Zweifach-Fung effect,[3] particles are attracted to the low flow rate side of a branch. Through experiment and modelling Doyeux *et al.* found that excluding a particular size particle from a branch may require a streamline width that is as much as 50% smaller than the particle radius. A second contributing reason is that the devices, as fabricated, were approximately 48 μm deep, as opposed to the 50 μm as designed. This increases the main channel resistance more than it does the branch channel resistance because the branches are only 25 μm wide. This increased main channel resistance will mean more fluid flow in the branches, increasing the critical size at each branch. Increased flow ratio at each branch should raise the overall filtration ratio. This explanation is supported by the measured F_R's being generally higher than the design values (Table 1).

The maximum designed dynamic range, defined as the largest particle that could pass divided by the smallest separated particle is 50 μm divided by 7.2 μm = 6.9. This can be increased significantly at the cost of reduced filtration ratio by making the main channel wider and deeper. This is a real advantage of BFF that other popular passive microfluidic separation systems, such as DLD,[15,16] and inertial[17] separations cannot match.

3.2 Fungal spore filtration

As a demonstration of the utility of the device we demonstrate its use to remove large debris from a solution of fungal spores intended for commercial production as a purified product. Normally the spore prep is filtered using a 20-micron nylon mesh filter then sorted on a flow cytometer. Fig. 7a shows the scatter plot of this preparation. Sorting takes place based on a gate drawn around the major grouping shown in Fig. 7b. Microscopic analysis of the spores gives a mean diameter of 4.4 ± 0.9 μm, however the solution contains significant debris, both larger and smaller than the spherical spores. The larger debris can be difficult to distinguish from the spores themselves by flow cytometry and may be included in the sorted product. We have used the 5 μm cut-off device to precisely remove these large debris objects. Fig. 7b shows that the solution collected from the filtered output has a significantly reduced number of large events (FSC > 500) that are outside the spore population gate. Prior to passing through the BFF device, 27% of large events are outside the spore gate, while after processing in the BFF device only 13% of large events are outside the gate. No clogging was observed in 12-minute runs.

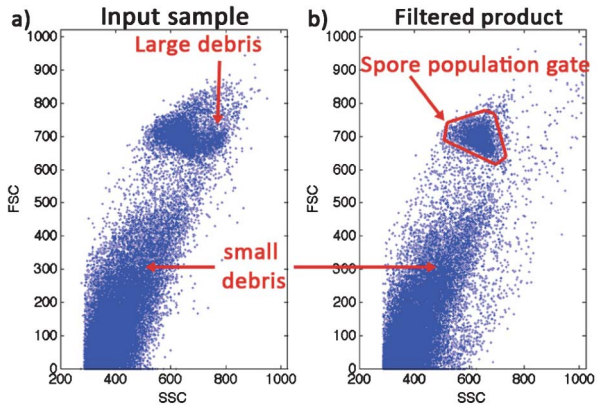

Fig. 7 Flow cytometry analysis of spore clean-up. Scatter plot of spore preparation before microdevice filtration (a) and after (b). Small debris is largely unaffected by the filter, as expected, but there is a significant reduction in large debris and the resulting solution has a more clearly defined spore populations.

4.0 Discussion

An obvious goal in this research is to achieve nano-scale resolution with inexpensive micron-sized features, while delivering high filtration rations and a sharp size cut-off. This is simply a matter of increasing the number of branches to increase the filtration ratio and appropriately lengthening the branches to reduce the size cut-off. Achieving this while retaining the sharp cutoff could possibly be achieved through a new analytical model that is not limited in terms of branch length or number, but it can also be achieved using the algorithm developed here on a more powerful computer.

While there is no fundamental limit to the sharpness of the filter, it is practically limited by variations in critical size at each branch and by stochastic particle–particle interactions. Fabrication errors such as thick or thin regions in the photoresist, particles and defects will also affect the branch widths and hence the amount of fluid flowing down each branch and thus the sharpness of the filter. Particle–particle interactions negatively affect sharpness because a high-density region of particles in one area will increase the apparent resistance of that path, lowering the fluid flow down that path, this phenomena is elegantly described by Fung 1973.[3] This effect is more significant at higher bead densities.

Another consideration affecting performance is inertial focussing.[17] The mean fluid velocity in the main channel ranged from 120 to 180 mm s^{-1} and the Reynold's number ranged from 9.6 to 6.6. We do not expect inertial focussing at this speed.

Finally we add that a common approach to treat this problem is to use a resistor network approximation. In this method each channel is represented as a fluidic resistor. The resistance can be calculated using an exact, explicit equation, derived from the solution to Navier–Stokes equation for a rectangular channel.[13] The fluidic network is replaced with a network of resistors where Kirchhoff's voltage and current laws are used to solve it with certain boundary conditions. We spent considerable effort on this approach and established that these models yield subtly different predictions from those obtained by our new method. These predictions, when solved as full 3D models had significant (>10%) variations in the cutoff size of each branch. We attribute the failure of this approach to the node resistances. In the resistor network approximation, the nodes (channel junctions) are assume to be of zero size and zero resistance, but as is clear in Fig. 1, the real nodes are of a similar size to the channels and their resistance can not be ignored. A second reason why this model may not be ideal is its failure to account for fluidic entrance lengths. Despite these problems the analytical model did provide significant insights into the design, including the requirement that the collection channel width increase as fluid is added to it.

5.0 Conclusion

We have presented a new approach to design branch flow fractionation devices that addresses limitations in previous work including low volume throughput, inconsistent cutoff sizes at branches, and large dead volumes. We produced microfluidic channel network designs by iteratively changing the geometry of a 3D CFD model. These designs were then realized by conventional microfluidic techniques and characterized by measuring the depletion of a range of polymer beads from 5 to 15 μm in diameter. Filtration ratios were within a few per-cent of designed-for values, while cut-off sizes were significantly larger than designed-for values. The devices achieved very precise fractionation (10× depletion for 12% size difference) while maintaining a high dynamic range (6.9) and a comparatively high filtration ratio (14%). Filter sharpness was high, with large particle rejection fitting a 20th order Butterworth filter. This characterization validates the novel design approach.

The design approach can be scaled to larger filtration ratios and smaller cutoff sizes with improved computer resources and expertise. The approach can easily be modified to include insights gained from fundamental studies of particle-branch interactions, like those in reference[10] which describing differences in cutoff size and stream width. The approach is highly compatible with low cost manufacturing processes as the minimum feature size can be set to the manufacturing requirement and manufacturing realities like draft angle and feature radii can be included without affecting the iterative method. This approach solves the problem of increasing the filtration ratio without overly large dead volumes or sacrificing filter sharpness.

Acknowledgements

The author thanks Dr Robert Nordon and Prof. Ben Goldys at the University of New South Wales for input and guidance in developing and solving resistor network models of the device. The author thanks Professor Ewa Goldys at Macquarie University for her effort throughout. This work was funded by the Australian Research Council (DP110102207) and Macquarie University.

References

1 M. Yamada and M. Seki, Hydrodynamic filtration for on-chip particle concentration and classification utilizing microfluidics, *Lab Chip*, 2005, **5**, 1233–1239.
2 N. Pamme, Continuous flow separations in microfluidic devices, *Lab Chip*, 2007, **7**, 1644–1659.
3 Y. Fung, Stochastic flow in capillary blood vessels, *Microvasc. Res.*, 1973, **5**, 34–44.
4 M. Yamada and M. Seki, Microfluidic particle sorter employing flow splitting and recombining, *Anal. Chem.*, 2006, **78**, 1357–1362.

5 Z. Y. Yan, A. Acrivos and S. Weinbaum, A three-dimensional analysis of plasma skimming at microvascular bifurcations, *Microvasc. Res.*, 1991, **42**, 17–38.
6 R. D. Jaggi, R. Sandoz and D. S. Effenhauser, Microfluidic depletion of red blood cells from whole blood in high-aspect-ratio microchannels, *Microfluid. Nanofluid.*, 2007, **3**, 47–53.
7 S. Yang, A. Ündar and J. D. Zahn, A microfluidic device for continuous, real time blood plasma separation, *Lab Chip*, 2006, **6**, 871–880.
8 S. Zheng, J. Liu and Y. Tai, Streamline-based microfluidic devices for erythrocytes and leukocytes separation, *J. Microelectromech. Syst.*, 2008, **17**, 1029–1038.
9 E. Sollier, M. Cubizolles, Y. Fouillet and J. Achard, Fast and continuous plasma extraction from whole human blood based on expanding cell-free layer devices, *Biomed. Microdevices*, 2010, **12**, 485–497.
10 V. Doyeux, T. Podgorski, S. Peponas, M. Ismail and G. Coupier, Spheres in the vicinity of a bifurcation: elucidating the Zweifach-Fung effect, *J. Fluid Mech.*, 2001, **674**, 359–388.
11 X. Xue, S. Marson, M. K. Patel, C. Bailey, W. O'Neill, D. Topham, R. W. Kay and M. P. Y. Desmulliez, Progress towards the design and numerical analysis of a 3D microchannel biochip separator., *Int. J. Numer. Meth. Biomed. Eng.*, 2011, **27**, 1771–1792.
12 P. Sethu, A. Sin and M. Toner, Microfluidic diffusive filter for apheresis (leukapheresis), *Lab Chip*, 2005, **5**, 83–89.
13 D. W. Inglis, A method for reducing pressure-induced deformation in silicone microfluidics, *Biomicrofluidics*, 2010, **4**, 024109.
14 L. R. Huang, E. C. Cox, R. H. Austin and J. C. Sturm, *Science*, 2004, **304**, 987–990.
15 D. W. Inglis, J. A. Davis, R. H. Austin and J. C. Sturm, *Lab Chip*, 2006, **6**, 655–658.
16 D. Di Carlo, D. Irimia, R. G. Tompkins and M. Toner, *Proc. Natl. Acad. Sci. U. S. A.*, 2007, **104**, 18892–18897.
17 J. P. Brody, P. Yager, R. E. Goldstein and R. H. Austin, Biotechnology at low Reynolds numbers, *Biophys. J.*, 1996, **71**, 3430–3441.